FOI
SWEDISH DEFENCE
RESEARCH AGENCY

FOI-R--0459--SE
March 2002
ISSN 1650-1942
Methodology report

Transparent boundary conditions for parabolic equations in underwater acoustics

Peter Karlsson

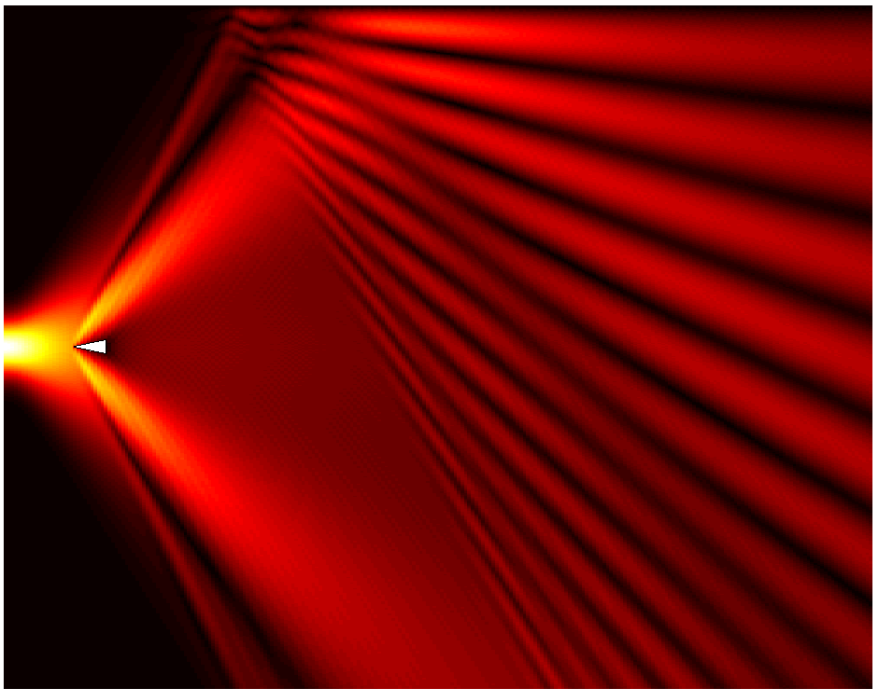

Systems Technology
SE-17290 Stockholm

SWEDISH DEFENCE RESEARCH AGENCY
Systems Technology
SE-172 90 Stockholm

FOI-R--0459--SE
March 2002
ISSN 1650-1942
Methodology report

Transparent boundary conditions for parabolic equations in underwater acoustics

Peter Karlsson

Issuing organization	Report number, ISRN	Report type
FOI – Swedish Defence Research Agency Systems Technology SE-172 90 Stockholm	FOI-R--0459--SE	Methodology report
	Research area code 4. C4ISR	
	Month year March 2002	**Project no.** E6051
	Customers code 1. Research for the Government	
	Sub area code 43 Underwater Sensors	
Author/s (editor/s) Peter Karlsson	**Project manager** Johan Mattsson	
	Approved by	
	Sponsoring agency Swedish Armed Forces	
	Scientifically and technically responsible Leif Abrahamsson	

Report title

Transparent boundary conditions for parabolic equations in underwater acoustics

Abstract (not more than 200 words)

In this thesis the creation of discrete transparent boundary conditions (DTBC's) for parabolic wave equations (PE's) in underwater acoustics is treated. The DTBC's are obtained by using analytical solutions to PE's for a semi-infinite and homogeneous bottom. These new boundary conditions have been compared with the method of damping layers, which until recently was the common way to truncate an infinite bottom. Three testing examples were used for the evaluation: the Lloyd mirror, the Bucker wave-guide and the Jensen-Kuperman wedge. We used three different damping profiles in the evaluation, two linear and one non-linear. The DTBC's showed to be much more time efficient and correct than the damping layer method.

A first display of the functionality of the DTBC can be seen on the front page, which shows the evolution of a beam hitting a wedge shaped prism in a homogeneous water half-space. As seen from the figure the part of the beam that encounters the surface is reflected back while the bottom boundary is transparent.

Keywords

SPE, WAPE, TBC, DTBC, transparent boundary conditions, underwater acoustics, wave propagation model

Further bibliographic information	**Language** English
ISSN 1650-1942	**Pages** 36 p.
	Price acc. to pricelist

Utgivare	Rapportnummer, ISRN	Klassificering
Totalförsvarets Forskningsinstitut - FOI Systemteknik 172 90 Stockholm	FOI-R--0459--SE	Metodrapport
	Forskningsområde 4. Spaning och ledning	
	Månad, år Mars 2002	**Projektnummer** E6051
	Verksamhetsgren 1. Forskning för regeringens behov	
	Delområde 43 Undervattenssensorer	

Författare/redaktör	Projektledare
Peter Karlsson	Johan Mattsson
	Godkänd av
	Uppdragsgivare/kundbeteckning Försvarsmakten
	Tekniskt och/eller vetenskapligt ansvarig Leif Abrahamsson

Rapportens titel (i översättning)

Transparenta randvillkor för paraboliska ekvationer i undervattensakustik

Sammanfattning (högst 200 ord)

I denna rapport behandlas skapandet av diskreta transparenta randvilkor för paraboliska ekvationer inom undervattensakustik. De diskreta randvilkoren är framtagna genom att analytiskt lösa de paraboliska ekvationerna för en halv-oändlig homogen botten. Dessa nya randvilkor har jämförts med användandet av en ”falsk botten”, vilket hittills varit det vanligaste sättet att trunkera en oändlig botten. Tre testexempel användes vid utvärderingen: Lloyd Mirror, Bucker wave-guide och Jensen-Kuperman wedge. För den ”falska botten” använde vi tre olika dämpningsprofiler, två linjära samt en ickelinjär. De diskreta randvilkoren visade sig vara mycket mer tidseffektiva och korrekta än den ”falska botten”.

På framsidan ges ett första exempel på funktionaliteten hos de diskreta randvilkoren, vilken visar hur en stråle sprids mha ett kilformat prisma. Som synes i figuren reflekteras den del av strålen som träffar ytan medan den nedre gränsen är transparent.

Nyckelord

SPE, WAPE, TBC, DTBC, transparenta randvilkor, undervattensakustik, vågutbredningsmodell

Övriga bibliografiska uppgifter	Språk Engelska
ISSN 1650-1942	**Antal sidor:** 36 s.
Distribution enligt missiv	**Pris: Enligt prislista**

Contents

1 Introduction

The parabolic wave equations (PE's), which this paper is built upon, were first used in the 1940s within radio wave propagation in the atmosphere. Since then the field of use has been extended (seismology, optics, plasma physics), and in the early 1970s Hardin and Tappert [1] started to use PE's in underwater acoustics. Today it is one of the most important wave propagation models in underwater acoustics [3], [7] and [9]. Several theoretical and applied works on PE's have been carried out at FOI e.g. [10-14], and this thesis is part of an ongoing development of PE models at FOI.

PE's are approximations to the classical wave equation, or the Helmholtz equation for mono-frequency sound fields. PE-models rely on the presence of a predominant direction of wave propagation. In underwater acoustics this direction is horizontal with a small angular spread in the vertical plane. For the two most common PE's, the standard parabolic equation (SPE) and the wide-angle parabolic equation (WAPE), the propagation angles around the horizontal plane should be less than 15° and 40° respectively. As is customary in underwater acoustics we shall assume that the fields are azimuthally symmetric around the source in the horizontal plane, which justifies calculations in two dimensions (2D).

Here a 2D coordinate system will be used, where x is the horizontal axis and z is the vertical, counted positive downward going through the source, see Figure 1. The physical problem is posed on the unbounded z-interval $(-\infty, \infty)$, while one usually is interested in the solution in the water and sometimes a little bit into the bottom. This is achieved by applying a Dirichlet (pressure release) boundary condition (BC) at the surface. However, there is no well-defined lower boundary on which a value of pressure (or velocity) can be specified. A standard strategy to cope with this is to introduce an absorbing layer terminated by a Dirichlet BC. This artificial damping layer costs lots of "unnecessary" computation and can cause reflections when using a less correct damping profile. There exist many ideas of how to get an optimal damping profile, but without a correct half-space solution, it's hard to say which one to use or how much it modifies the correct solution.

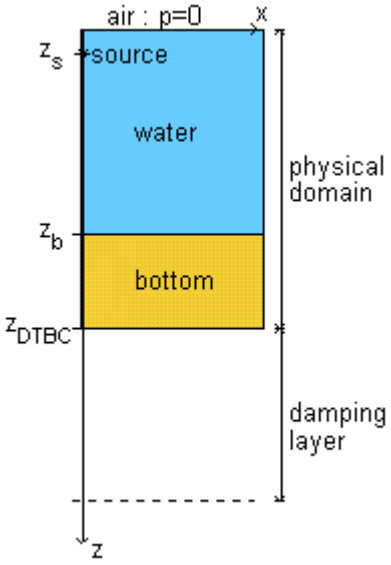

Figure 1 Sketch of the general solution domain.

The need for a "false bottom" can be eliminated by the use of a transparent boundary condition (TBC), which allows waves to leave the computational domain without backscattering. Such a BC simulates the acoustic response of a homogeneous, half-infinite bottom. This BC is usually applied at a horizontal interface $z = z_{DTBC}$ such that the bottom below is homogeneous. The chief advantage is that the depth wise extension $0 \leq z \leq z_{DTBC}$ is much less then using absorbing layers. The first one to formulate a TBC for the SPE in underwater acoustics was Papadakis [15], whose work has been followed by several others [16] and [17]. Recently Arnold and Ehrhardt [2] introduced a somewhat new approach. They constructed discrete transparent boundary conditions (DTBC's) by solving the finite difference equation for SPE and WAPE for a homogeneous

half-infinite bottom. It implies that they are equivalent to solving the discrete equation over a half-infinite domain. This approach ensures complete transparency and stability. The disadvantage is that the step-size in range must be uniform.

The purpose with this thesis is:

- implement DTBC's
- validate the performance of DTBC's on a set of reference problems
- make comparisons with the absorbing layer approach regarding accuracy and computational efficiency

Our approach when constructing the DTBC's is similar to what Arnold and Ehrhardt does in [2], and implies an analytical solution of the PE's in the bottom half-space. This DTBC can then be applied immediately at the water bottom interface, or a bit down into the bottom, resulting in the correct solution in the restricted domain $z \in (0, z_{DTBC})$, where z_{DTBC} is the depth where one chooses to cut the computational domain.

The results from this thesis can be summarised as follows:

- DTBC's have worked excellently on all test examples
- the computational cost is significantly less with DTBC's versus absorbing layers if the step-range is uniform
- the accuracy of the DTBC solutions are much better then the ones obtained with damping layers

2 Theory

In this chapter we will derive the transparent boundary conditions (TBC's), with the Helmholtz equation as starting point.

2.1 Derivation of the SPE and WAPE approximations

Hydrodynamic and adiabatic relations between pressure and density leads to the acoustic wave equation in an ideal fluid, which for time-harmonic fields ($p \propto e^{-i\omega t}$) leads to the Helmholtz equation:

$$\rho \frac{\partial}{\partial x}\left(\frac{1}{\rho}\frac{\partial p}{\partial x}\right)+\rho \frac{\partial}{\partial z}\left(\frac{1}{\rho}\frac{\partial p}{\partial z}\right)+k^2 p=0\,. \qquad \textbf{(1)}$$

The variables in the equation above and the ones used later on in this section are defined in Table 1.

Table 1 Definition of used variables.

Variable	Definition	Unit
p	Acoustic pressure	Pa
ρ	Density	kg/m^3
k	$\frac{\omega}{c}\left(1+i\frac{\delta}{4\pi\log(e)}\right)$, complex wave number	m^{-1}
ω	2πf, angular velocity	rad/s
f	Frequency	Hz
c	Velocity of sound	m/s
δ	Absorption	dB/λ
λ	c/f, wavelength	m

Using the mathematical identity

$$\rho \frac{\partial}{\partial x}\left(\frac{1}{\rho}\frac{\partial p}{\partial x}\right)=\rho \frac{\partial^2}{\partial x^2}\left(\frac{1}{\rho}p\right)+\underbrace{\frac{1}{2}\sqrt{\rho}\,\frac{\partial}{\partial x}\left(\frac{1}{\rho^{3/2}}\frac{\partial \rho}{\partial x}\right)p}_{\approx 0}\,, \qquad \textbf{(2)}$$

and assuming that the second derivative of the density, at the right hand side (RHS), is negligible, i.e. small density fluctuations in x, Eq. (1) becomes

$$\left(\frac{\partial^2}{\partial x^2}+\sqrt{\rho}\,\frac{\partial}{\partial z}\left(\frac{1}{\rho}\frac{\partial}{\partial z}\sqrt{\rho}\right)+k^2\right)p_\rho=0, \qquad \textbf{(3)}$$

where $p_\rho=\frac{1}{\sqrt{\rho}}p$.

Factoring the operators in the above equation into a product of outgoing and incoming operators gives

$$\underbrace{(P-iQ)}_{out}\underbrace{(P+iQ)}_{in}p_\rho-i[P,Q]p_\rho=0, \qquad \textbf{(4)}$$

where

$$P=\frac{\partial}{\partial x},$$

$$Q=\sqrt{k^2+\sqrt{\rho}\,\frac{\partial}{\partial z}\left(\frac{1}{\rho}\frac{\partial}{\partial z}\sqrt{\rho}\right)}.$$

The commutator term vanishes when the media parameters are range-independent. Otherwise we need to assume that the range dependence is so weak that it can be neglected. We can now write down the parabolic wave equation (PE) also known as the one-way approximation,

$$(P-iQ)p_\rho=0. \qquad \textbf{(5)}$$

Introducing the reference wave number $k_0=\frac{\omega}{c_0}$, where c_0 usually is the lowest sound velocity of the water, and rewriting the square root operator, Q, as

$$\sqrt{k^2+\sqrt{\rho}\,\frac{\partial}{\partial z}\left(\frac{1}{\rho}\frac{\partial}{\partial z}\sqrt{\rho}\right)}=k_0\sqrt{1+q}, \qquad \textbf{(6)}$$

where

$$q=\frac{k^2-{k_0}^2}{{k_0}^2}+\frac{1}{{k_0}^2}\sqrt{\rho}\,\frac{\partial}{\partial z}\left(\frac{1}{\rho}\frac{\partial}{\partial z}\sqrt{\rho}\right)$$

the PE can be written in the more compact form

$$\left(\frac{\partial}{\partial x}-ik_0\sqrt{1+q}\right)p_\rho=0. \qquad \textbf{(7)}$$

By approximating $\sqrt{1+q}$ with the Taylor expansion of the first degree, $1+\frac{1}{2}q$, and with the more accurate rational approximation $\frac{p_0 + p_1 q}{1+p_2 q}$, one get the standard parabolic equation (SPE) and the wide-angle parabolic equation (WAPE). Here the values of the constants p_0, p_1 and p_2 will be set to 1, 0.75 and 0.25, the so called Claerbout approximation. The approximated equations can now, substituting back the pressure variable, be written as

SPE:

$$\frac{\partial}{\partial x}\left(\frac{p}{\sqrt{\rho}}\right) - \frac{i}{2k_0}\sqrt{\rho}\frac{\partial}{\partial z}\left(\frac{1}{\rho}\frac{\partial}{\partial z}p\right) - \frac{i\alpha p}{\sqrt{\rho}} = 0 \qquad \textbf{(8)}$$

where

$$\alpha = \frac{k^2 + {k_0}^2}{2k_0}$$

WAPE:

$$\sqrt{\rho}\frac{\partial}{\partial z}\left(\frac{1}{\rho}\frac{\partial}{\partial z}\left(\sqrt{\rho}\frac{\partial}{\partial x}\left(\frac{p}{\sqrt{\rho}}\right)\right)\right) + \beta\frac{\partial}{\partial x}\left(\frac{p}{\sqrt{\rho}}\right) + i\chi\frac{p}{\sqrt{\rho}} + i\gamma\sqrt{\rho}\frac{\partial}{\partial z}\left(\frac{1}{\rho}\frac{\partial p}{\partial z}\right) = 0 \qquad \textbf{(9)}$$

where

$$\beta = k^2 + 3{k_0}^2,$$
$$\chi = -k_0(3k^2 + {k_0}^2),$$
$$\gamma = -3k_0.$$

The SPE can be shown to be a good approximation of wave propagation in the far field within a 15-degree angle from the horizontal, and the WAPE works up to 40 degrees [3].
A common way to make it possible to increase the step size in the numerical scheme is to reduce the wave dependence in the propagating direction, and calculate with the envelopes. This is achieved by substituting p with $ue^{ik_0 x}$, which gives the base equations that this thesis is built upon

SPE_{env}:

$$\frac{\partial}{\partial x}\left(\frac{u}{\sqrt{\rho}}\right) - \frac{i}{2k_0}\sqrt{\rho}\frac{\partial}{\partial z}\left(\frac{1}{\rho}\frac{\partial}{\partial z}u\right) - \frac{i\alpha_{env}u}{\sqrt{\rho}} = 0 \qquad \textbf{(10)}$$

where

$$\alpha_{env} = \frac{k^2 - {k_0}^2}{2k_0}$$

and

WAPE$_{env}$:

$$\sqrt{\rho}\,\frac{\partial}{\partial z}\left(\frac{1}{\rho}\frac{\partial}{\partial z}\left(\sqrt{\rho}\,\frac{\partial}{\partial x}\left(\frac{u}{\sqrt{\rho}}\right)\right)\right) + \beta_{env}\,\frac{\partial}{\partial x}\left(\frac{u}{\sqrt{\rho}}\right) + i\chi_{env}\,\frac{u}{\sqrt{\rho}} + i\gamma_{env}\sqrt{\rho}\,\frac{\partial}{\partial z}\left(\frac{1}{\rho}\frac{\partial u}{\partial z}\right) = 0 \qquad \textbf{(11)}$$

where

$$\beta_{env} = k^2 + 3{k_0}^2,$$
$$\chi_{env} = 2k_0({k_0}^2 - k^2),$$
$$\gamma_{env} = -2k_0.$$

Hereafter the index env will be dropped and all further calculations will be done with the envelopes.

2.2 Construction of discrete transparent boundary conditions

When constructing the DTBC, the media parameters in the bottom below z_{DTBC} are assumed to be constant, which leads to the following simplifications of Eq. (10) and (11),

SPE:

$$\frac{\partial u}{\partial x} - \frac{i}{2k_0}\frac{\partial^2 u}{\partial z^2} - i\alpha u = 0, \qquad x \geq 0,\ z \geq z_{DTBC} \qquad \textbf{(12)}$$

WAPE:

$$\frac{\partial^2}{\partial z^2}\left(\frac{\partial u}{\partial x}\right) + \beta\frac{\partial u}{\partial x} + i\chi u + i\gamma\frac{\partial^2 u}{\partial z^2} = 0, \qquad x \geq 0,\ z \geq z_{DTBC}. \qquad \textbf{(13)}$$

In this section the envelope equations, for the SPE and WAPE approximations, will be solved in the bottom half-space for the three cases; continuous, discrete in x and discrete in both x and z. The semi-discretization is made to simplify the analysis of comparison between the continuous and fully discretized case.

The continuity conditions at the interface z_{DTBC} are given by

$$p(z_{DTBC-}, x) = p(z_{DTBC+}, x), \tag{14}$$

$$\frac{1}{\rho^{DTBC-}} \frac{\partial p(z_{DTBC-}, x)}{\partial z} = \frac{1}{\rho^{DTBC+}} \frac{\partial p(z_{DTBC+}, x)}{\partial z}, \tag{15}$$

where the minus stands for the variable value just above z_{DTBC} and the plus for the value just below. Eq. (14) says that the pressure is continuous and Eq. (15) states the continuity of particle velocity in the z direction at the boundary.

2.2.1 Solving the continuous SPE

For notational convenience we assume that $z_{DTBC} = 0$. We shall also assume that $u(0,z) = 0$ for $z \geq 0$. To make Eq. (12) easier to solve it is transformed to the Laplace space,

$$\frac{\partial^2 \hat{u}(s,z)}{\partial z^2} + i2k_0(s - i\alpha)\hat{u}(s,z) = 0 , \qquad z \geq 0. \tag{16}$$

The solution to this equation, if assuming the solution to be bounded at $z = \infty$ and that the initial condition $\hat{u}(s,0)$ is given, can be written

$$\hat{u}(s,z) = \hat{u}(s,0) e^{i * \sqrt{i2k_0(s - i\alpha)} * z}, \tag{17}$$

where the imaginary part of the square root must be larger than zero for the solution to be bounded. If we differentiate the above solution with respect to z and set z=0, Eq. (17) will be

$$\frac{\partial \hat{u}(s,0)}{\partial z} = \hat{u}(s,0) i * \sqrt{2ik_0(s - i\alpha)} . \tag{18}$$

By using the inverse Laplace transform formulas [8]

$$L^{-1}\left\{ \frac{1}{\sqrt{s - i\alpha}} \right\} = \frac{1}{\sqrt{\pi x}} e^{i\alpha x}, \tag{19}$$

$$L^{-1}\{(s - i\alpha)\hat{u}(s,0)\} = \frac{\partial u(x,0)}{\partial x} - i\alpha u(x,0), \tag{20}$$

the boundary condition (18) can be expressed as a convolution,

$$\frac{\partial u(x,0)}{\partial z} = -\sqrt{\frac{k_0}{\pi}}\left(\frac{2}{1+i}\right)\int_0^x \left\{\left(\frac{\partial u(\tau,0)}{\partial \tau} - i\alpha u(\tau,0)\right)\frac{1}{\sqrt{x-\tau}} e^{i\alpha(x-\tau)}\right\} d\tau . \qquad \textbf{(21)}$$

It means that any solution to the SPE in the region $x \geq 0$, $z \geq 0$ will satisfy the BC in Eq. (21). Together with the matching conditions in Eq. (14) and Eq. (15), it permits waves to enter the region $z \geq 0$ without any backreflection.

The BC in Eq. (21) is non-local in the sense that the convolution integral involves the entire solution at the boundary from $x = 0$ up to the point where the BC is applied. Due to the causal nature of the PE this solution can be considered as known.

The above derivation also appears in [16], where it was applied to parabolic models of water waves.

2.2.2 Solving the semi-discrete SPE

We introduce a uniform grid $x^n = n\Delta x$ ($n = 0, 1, 2\ldots$) while the z-variable is kept continuous. The corresponding semi-discrete solution is denoted by $u^n(z)$. Discretizing Eq. (12) in x, with the Crank-Nicolson algorithm [5], leads to

$$\frac{u^{n+1}(z) - u^n(z)}{\Delta x} = \frac{i}{4k_0}\left[\frac{\partial^2 u^{n+1}(z)}{\partial z^2} + \frac{\partial^2 u^n(z)}{\partial z^2}\right] + \frac{i\alpha}{2}\left[u^{n+1}(z) + u^n(z)\right]. \qquad \textbf{(22)}$$

Transforming Eq. (22) with the Z-transform,

$$\hat{u}(\zeta, z) = \sum_{n=0}^{\infty} u^n(z)\zeta^{-n} , \qquad \textbf{(23)}$$

gives

$$\frac{\zeta - 1}{\Delta x}\hat{u}(\zeta, z) = \frac{i}{4k_0}(\zeta + 1)\frac{\partial^2 \hat{u}(\zeta, z)}{\partial z^2} + \frac{i\alpha}{2}(\zeta + 1)\hat{u}(\zeta, z) . \qquad \textbf{(24)}$$

Solving Eq. (24), and as in the continuous case, assuming the solution to be bounded at $z = \infty$ and with a initial condition $\hat{u}(\zeta, 0)$, the solution can be written

$$\hat{u}(\zeta, z) = \hat{u}(\zeta,0)e^{i*\sqrt{2k_0\alpha + \frac{i4k_0(\zeta-1)}{\Delta x(\zeta+1)}}*z}. \quad \textbf{(25)}$$

Differentiate with respect to z and set z=0, Eq. (25) can be rewritten as

$$\frac{\partial \hat{u}(\zeta,0)}{\partial z} = \hat{u}(\zeta,0)i2k_0 \frac{\alpha(\zeta+1) + \frac{2i}{\Delta x}(\zeta-1)}{\sqrt{A_{SPE\_x}\zeta^2 + B_{SPE\_x}\zeta + C_{SPE\_x}}}, \quad \textbf{(26)}$$

where

$$A_{SPE\_x} = 2k_0\alpha + \frac{4ik_0}{\Delta x},$$
$$B_{SPE\_x} = 4k_0\alpha \text{ and}$$
$$C_{SPE\_x} = 2k_0\alpha - \frac{4ik_0}{\Delta x}.$$

Now using the mathematical identity that the inverse square root can be written as a sum of Legendre polynomials [6]

$$\frac{1}{\sqrt{1 - \frac{2\mu}{\zeta} + \frac{1}{\zeta^2}}} = \sum_{n=0}^{\infty} P_n(\mu)\left[\frac{1}{\zeta}\right]^n, \quad \textbf{(27)}$$

the inverse transform takes the form

$$\mathrm{Z}^{-1}\left\{\frac{1}{\sqrt{1 - \frac{2\mu}{\zeta} + \frac{1}{\zeta^2}}}\right\} = P_n(\mu). \quad \textbf{(28)}$$

Using the above relation together with

$$\mathrm{Z}^{-1}\left\{\frac{\partial \hat{u}(\zeta,0)}{\partial z}\zeta\right\} = \frac{\partial u^{n+1}(0)}{\partial z}, \quad \textbf{(29)}$$

$$\mathrm{Z}^{-1}\{(\zeta \pm 1)\hat{u}(\zeta,0)\} = \frac{u^{n+1}(0) \pm u^n(0)}{\Delta x}, \quad \textbf{(30)}$$

the Eq. (26) can be inverse transformed to

$$\frac{\partial u^{n+1}(0)}{\partial z} = \frac{-4k_0}{\sqrt{A_{SPE\_x}}} \sum_{k=0}^{n} l_{n-k} \left(\frac{u^{n+1}(0) - u^n(0)}{\Delta x} - \frac{i\alpha}{2}\left(u^{n+1}(0) + u^n(0)\right) \right), \tag{31}$$

where the weights l_{n-k} are defined by

$$l_{n-k} = P_{n-k}(\mu) \left(\sqrt{\frac{C_{SPE\_x}}{A_{SPE\_x}}} \right)^{n-k}, \tag{32}$$

and μ is given by

$$\mu = -\frac{B_{SPE\_x}}{2\sqrt{A_{SPE\_x} C_{SPE\_x}}}. \tag{33}$$

Eq. (31) is the semi-discrete transparent boundary condition, which corresponds to the continuous one given by Eq. (21) but with the integral replaced by a sum.

2.2.3 Solving the fully discrete SPE

After this point it's time to make the full discretization of the SPE. Starting with the semi-discretized Eq. (23) and discretizing it in z with $z_j = j\Delta z$ (j = 0, 1, 2…) gives

$$\frac{u_j^{n+1} - u_j^n}{\Delta x} = \frac{i}{4k_0} \left(\frac{u_{j+1}^{n+1} - 2u_j^{n+1} + u_{j-1}^{n+1}}{\Delta z^2} + \frac{u_{j+1}^{n} - 2u_j^{n} + u_{j-1}^{n}}{\Delta z^2} \right) + \frac{i\alpha}{2}\left(u_j^{n+1} + u_j^n\right). \tag{34}$$

Z-transforming the above equation in x and rearranging, gives the difference equation

$$\hat{u}_{j+1}(\zeta) + 2(\sigma - 1)\hat{u}_j(\zeta) + \hat{u}_{j-1}(\zeta) = 0,$$

where σ is defined by

$$\sigma = \frac{2k_0\Delta z^2}{\zeta + 1} \left\{ \left(\alpha + \frac{2i}{\Delta x} \right)\zeta + \alpha - \frac{2i}{\Delta x} \right\}. \tag{35}$$

The solution to Eq. (35) is now, assuming the initial condition $\hat{u}_0$ to be given,

$$\hat{u}_j(\zeta) = \gamma^j \hat{u}_0(\zeta), \tag{36}$$

where γ is defined according to

$$\gamma = 1 - \sigma \pm \sqrt{\sigma^2 - 2\sigma}$$

and demands it to be limited, as $|\gamma| < 1$. This since the modes should decrease, which leads to the ignoring of the negative sign of the square root. Now the derivative is constructed

$$\frac{\hat{u}_1 - \hat{u}_0}{\Delta z} = \frac{1}{\Delta z}\frac{\gamma - 1}{\gamma + 1}(\hat{u}_0 + \hat{u}_1). \tag{37}$$

Eq. (37) can in full be written as

$$\frac{\hat{u}_1 - \hat{u}_0}{\Delta z} = \frac{ik_0\Delta z\left(\left(\alpha + \frac{2i}{\Delta x}\right)\zeta + \alpha - \frac{2i}{\Delta x}\right)(\hat{u}_0 + \hat{u}_1)}{\sqrt{A_{SPE\_xz}\zeta^2 + B_{SPE\_xz}\zeta + C_{SPE\_xz}}}, \tag{38}$$

where

$$A_{SPE\_xz} = 2k_0\left(\alpha + \frac{2i}{\Delta x}\right) - k_0^2\Delta z^2\left(\alpha + \frac{2i}{\Delta x}\right)^2,$$
$$B_{SPE\_xz} = 4k_0\alpha - 2k_0^2\Delta z^2\left(\alpha^2 + \frac{4}{\Delta x^2}\right),$$
$$C_{SPE\_xz} = 2k_0\left(\alpha - \frac{2i}{\Delta x}\right) - k_0^2\Delta z^2\left(\alpha - \frac{2i}{\Delta x}\right)^2.$$

Using the same method as in the semi-discrete case, the inverse transform of Eq. (38), takes the form

$$\frac{u_1^{n+1} - u_0^{n+1}}{\Delta z} = \frac{-4k_0}{\sqrt{A_{SPE\_xz}}}\sum_{k=0}^{n} l_{n-k}\left(\frac{u_0^{k+1} - u_0^k + u_1^{k+1} - u_1^k}{2\Delta x} - \frac{i\alpha}{4}\left(u_0^{k+1} + u_0^k + u_1^{k+1} + u_1^k\right)\right), \tag{39}$$

where the weights l_{n-k} is defined by Eq. (32) and (33), but with the index SPE_x changed to SPE_xz. This is the analogue of the continuous BC in Eq. (21), in which the convolution integral is replaced by a summation.

2.2.4 Solving the continuous WAPE

As for the SPE the WAPE, given by Eq. (13), is Laplace transformed

$$\frac{\partial^2 s\hat{u}}{\partial z^2} + \beta s\hat{u} + i\chi\hat{u} + i\gamma\frac{\partial^2 \hat{u}}{\partial z^2} = 0, \tag{40}$$

and using the same approach the solution is found to be

$$\frac{\partial \hat{u}(s,0)}{\partial z} = \frac{i\hat{u}(s,0)}{\sqrt{\beta}}\frac{\beta s + i\chi}{\sqrt{(s+a)^2 + b^2}}, \tag{41}$$

where

$$a = \frac{i(\beta\gamma + \chi)}{2\beta} \text{ and}$$

$$b = \frac{\beta\gamma - \chi}{2\beta}.$$

Using the inverse formula given by Eq. (23) and [8]

$$L^{-1}\left\{\frac{1}{\sqrt{(s+a)^2 + b^2}}\right\} = e^{-ax}J_0(bx), \tag{42}$$

where J_0 is the Bessel function of order zero, and the inverse transformed solution looks like follows

$$\frac{\partial u(x,0)}{\partial z} = i\sqrt{\beta}\int_0^x \left\{\left(\frac{\partial u(\tau,0)}{\partial \tau} - \frac{i\chi}{\beta}u(\tau,0)\right)e^{-a(x-\tau)}J_0(b(x-\tau))\right\}d\tau. \tag{43}$$

2.2.5 Solving the semi discrete WAPE

Discretizing Eq. (13) in x gives

$$\frac{\partial^2}{\partial z^2}\left(\frac{u^{n+1}(z)-u^n(z)}{\Delta x}\right)+\beta\left(\frac{u^{n+1}(z)-u^n(z)}{\Delta x}\right)+i\gamma\left(\frac{u^{n+1}(z)+u^n(z)}{2}\right)+$$
$$+i\chi\left(\frac{u^{n+1}(z)+u^n(z)}{2}\right)=0. \qquad \textbf{(44)}$$

Z-transforming the above equation, and solving it the same way as for the semi discrete SPE, and doing the same inverse transformation leads to the searched equation

$$\frac{\partial u^{n+1}(0)}{\partial z}=\frac{i\Delta x 2\beta}{\sqrt{A_{WAPE\_x}}}\sum_{k=0}^{n} l_{n-k}\left(\frac{u^{n+1}(0)-u^n(0)}{\Delta x}-\frac{i\chi}{2\beta}\left(u^{n+1}(0)+u^n(0)\right)\right), \qquad \textbf{(45)}$$

where the weights l_{n-k} is defined by Eq. (32) and (33), where the index SPE_x is changed to WAPE_x, and

$$A_{WAPE\_x}=4\beta-\Delta x^2\gamma\chi+i2\Delta x(\chi+\gamma\beta),$$
$$B_{WAPE\_x}=-8\beta-2\Delta x^2\gamma\chi \text{ and}$$
$$C_{WAPE\_x}=4\beta-\Delta x^2\gamma\chi-i2\Delta x(\chi+\gamma\beta).$$

2.2.6 Solving the fully discrete WAPE

The full discretization of Eq. (13) takes the form

$$\frac{1}{\Delta x\Delta z^2}\left\{u_{j+1}^{n+1}-2u_j^{n+1}+u_{j-1}^{n+1}-u_{j+1}^n+2u_j^n-u_{j-1}^n\right\}+\beta\left(\frac{u_j^{n+1}-u_j^n}{\Delta x}\right)+$$
$$+\frac{i\gamma}{2\Delta z^2}\left\{u_{j+1}^{n+1}-2u_j^{n+1}+u_{j-1}^{n+1}+u_{j+1}^n-2u_j^n+u_{j-1}^n\right\}+\frac{i\chi}{2}\left(u_j^{n+1}+u_j^n\right)=0. \qquad \textbf{(46)}$$

Doing the same procedure as for the fully discretized SPE, the solution can be written

$$\frac{u_1^{n+1}-u_0^{n+1}}{\Delta z}=\frac{i2\beta\Delta x}{\sqrt{A_{WAPE\_xz}}}\sum_{k=0}^{n} l_{n-k}\left(\frac{u_0^{k+1}-u_0^k+u_1^{k+1}-u_1^k}{2\Delta x}+\frac{i\chi}{4\beta}\left(u_0^{k+1}+u_0^k+u_1^{k+1}+u_1^k\right)\right), \qquad \textbf{(47)}$$

where the weights l_{n-k} is defined by Eqs. (32) and (33), where the index SPE_x is changed to WAPE_xz, and

$$A_{WAPE\_xz} = \beta\left(4-\beta\Delta z^2\right)+\Delta x^2\chi\left(\frac{\chi\Delta z^2}{4}-\gamma\right)+i\Delta x\left(2\chi+2\gamma\beta-\Delta z^2\chi\beta\right),$$

$$B_{WAPE\_xz} = -2\beta\left(4-\beta\Delta z^2\right)+2\left(\Delta x^2\chi\left(\frac{\chi\Delta z^2}{4}-\gamma\right)\right) \text{ and}$$

$$C_{WAPE\_xz} = \beta\left(4-\beta\Delta z^2\right)+\Delta x^2\chi\left(\frac{\chi\Delta z^2}{4}-\gamma\right)-i\Delta x\left(2\chi+2\gamma\beta-\Delta z^2\chi\beta\right).$$

3 Analyzing the convolution kernels

In this Chapter the kernels that were derived in the previous section, will be examined. The comparable convolution kernels of Eqs. (21), (33), (39), (43), (45) and (47) that will be used here are

$$-\sqrt{\frac{k_0}{\pi x}}\left(\frac{2}{1+i}\right)e^{i\alpha x}\Delta x, \qquad \text{(SPE continuous)} \qquad \textbf{(48)}$$

$$-\frac{4k_0}{\sqrt{A_{SPE\_x}}}l_n, \qquad \text{(SPE discrete in x)} \qquad \textbf{(49)}$$

$$-\frac{4k_0}{\sqrt{A_{SPE\_xz}}}l_n, \qquad \text{(SPE discrete in x and z)} \qquad \textbf{(50)}$$

$$i\sqrt{\beta}e^{-ax}J_0(bx)\Delta x, \qquad \text{(WAPE continuous)} \qquad \textbf{(51)}$$

$$\frac{i2\beta\Delta x}{\sqrt{A_{WAPE\_x}}}l_n \text{ and} \qquad \text{(WAPE discrete in x)} \qquad \textbf{(52)}$$

$$\frac{i2\beta\Delta x}{\sqrt{A_{WAPE\_xz}}}l_n. \qquad \text{(WAPE discrete in x and z)} \qquad \textbf{(53)}$$

3.1 Plotting and comparing the convolution kernels

At a first look at the kernels, it is interesting to note that the discretized SPE's are not singular at the origin, as the continuous one. Furthermore the kernels may be oscillating, setting the limit for the maximum step size, i.e. we have to sample with twice the oscillation frequencies to fully resolve the kernels.

Two main cases will be graphically investigated; one where the sound velocity is equal to the reference velocity, and the other case is when they differ. Some of the behaviors of the first case will be mathematically confirmed, while the other case is too complex, and therefore we will be satisfied with a graphical analysis.

Case 1:

Using a frequency of 100Hz, identical velocities for the sound in the bottom and the reference velocity (1500m/s), the following convolution kernels are achieved.

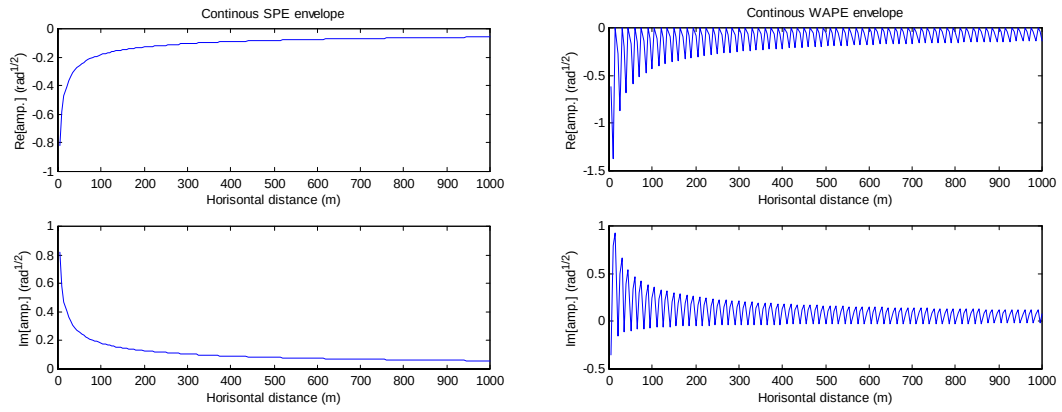

(a) **(b)**

Figure 2 The left figures (a) shows the behavior of the continuous convolution kernel for the SPE, and the right ones (b) correspond to the WAPE. The top panels are the real parts, and the bottom the imaginary.

The analytic expressions for the continuous SPE and WAPE are given by Eqs. (48) and (51), in which for case 1:

$$\alpha = 0, \qquad \text{(SPE)}$$

$$ia = -b = k_0 \text{ and} \qquad \text{(WAPE)}$$

$$k_0 = \frac{2\pi 100}{1500}.$$

We can see that both kernels decay slowly by range as $1/\sqrt{x}$. It implies that the solution at a short range may be important at a long range. The SPE kernel has a square-root singularity at x = 0 as opposed to the WAPE kernel. On the other hand the WAPE kernel oscillates with a wavenumber equal to k_0 while the SPE kernel is nonoscillatory. The kernel oscillation is a serious drawback because the solution itself is expected to be less oscillatory.

In Figures 3 and 4 we have compared the discrete and continuous kernels. The behavior of the discrete SPE's are somewhat unexpected, i.e. they are oscillating though the continuous is smooth. This behavior will be analytically confirmed for the semi-discrete case in Section 3.2. It is also seen that the Bessel expression, the continuous kernel for the WAPE, is not centered around zero, which a Bessel function usually is. This behavior is also looked at in the next section. There is a good agreement between the discrete and continuous WAPE kernels.

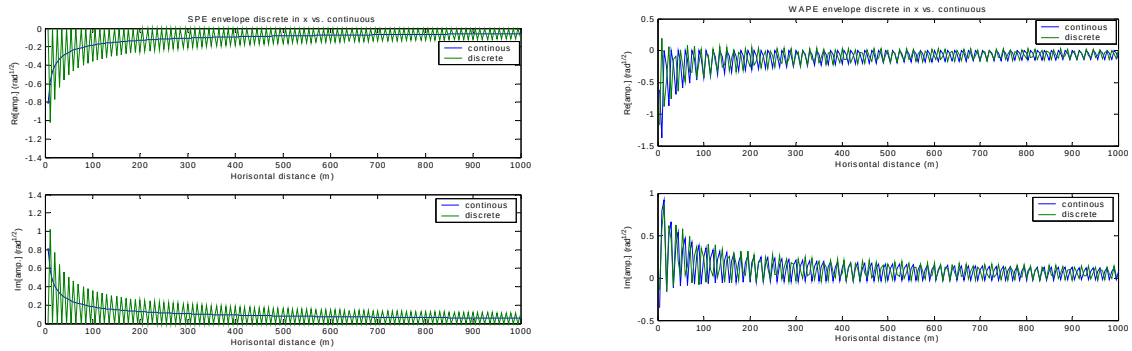

(a) **(b)**

Figure 3 The left panels (a) compares the real respectively the imaginary part for the semi discrete SPE and the continuous. The right ones (b) compares the same properties for the WAPE.

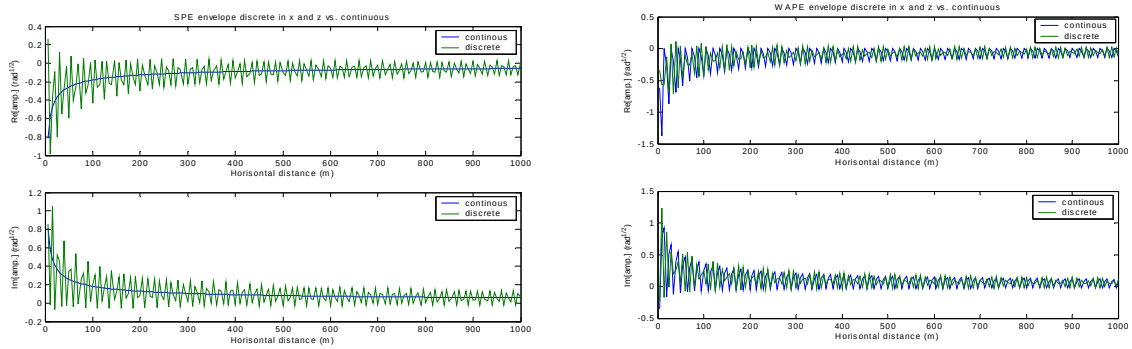

(a) **(b)**

Figure 4 The left panels (a) compares the real respectively the imaginary part for the fully discrete SPE and the continuous. The right ones (b) compares the same properties for the WAPE.

Case 2:

The only difference from case 1 is that the sound velocity is set to 1700m/s while the reference velocity is 1500m/s.

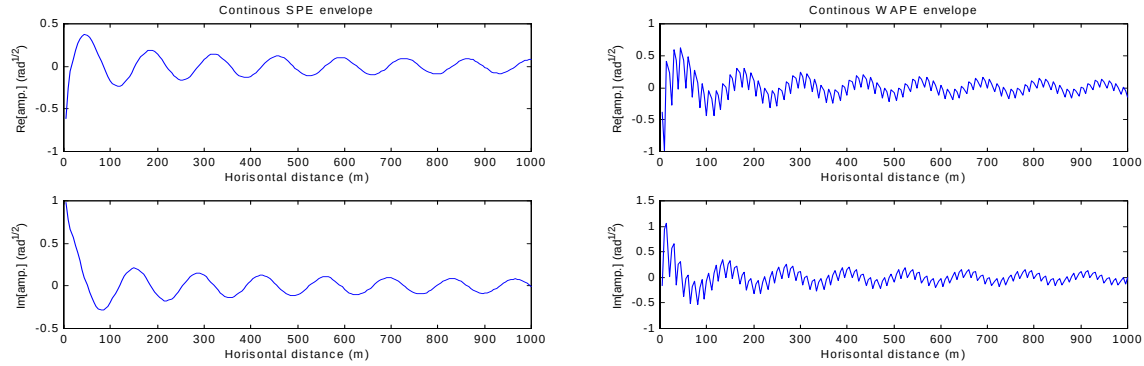

(a) **(b)**

Figure 5 The left panels (a) shows the behavior of the continuous convolution kernel for the SPE, and the right ones (b) correspond to the WAPE. The top figure is the real part, and the bottom the imaginary.

In opposite to the previous case the SPE kernel is now oscillatory. By looking at the analytic expressions in Eqs. (48) and (51) we find that

$$\alpha = \frac{k^2 - k_0^2}{2k_0}, \qquad \text{(SPE)}$$

$$ia = k_0 \frac{2\left(k^2 + k_0^2\right)}{k^2 + 3k_0^2}, \qquad \text{(WAPE)}$$

$$b = -k_0 \frac{4k_0^2}{k^2 + 3k_0^2}, \qquad \text{(WAPE)}$$

$$k_0 = \frac{2\pi 100}{1500} \text{ and}$$

$$k = \frac{2\pi 100}{1700}.$$

Approximately the oscillatory character of the kernels depends on the difference between the reference velocity and the sound velocity in the bottom. Again the WAPE kernel is less favourable since the rate of oscillation may be as large as $4k_0/3$ (when $k_0 >> k$).

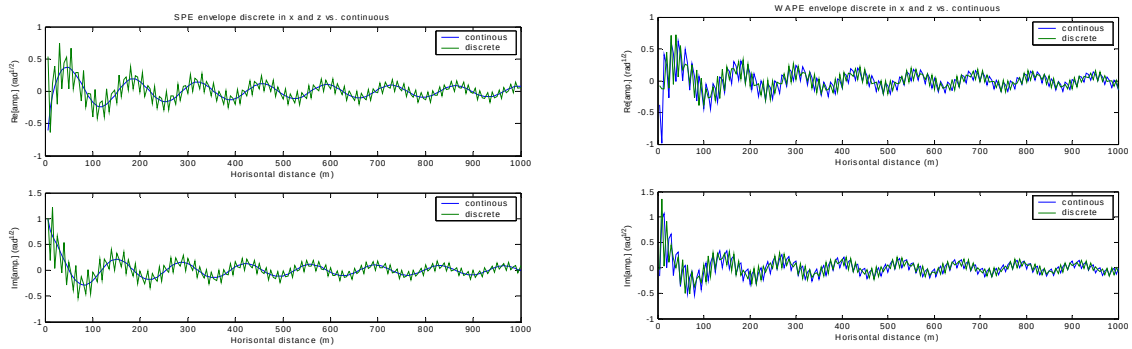

(a) **(b)**

Figure 6 The left panels compares the real respectively the imaginary part for the fully discrete SPE and the continuous. The right ones compares the same properties for the WAPE.

As can be seen in the Figs. 5 and 6 the main difference between case 2 and case 1 is that the kernel becomes more oscillatory in the second case. However, the behaviors and amplitudes are somewhat the same.

3.2 Analysis of kernels

In this section we will clarify some of the features of the kernels observed in Figure 3a and b. From the Figure 3b it was noticed that the kernel oscillation of the WAPE were not centered around zero. The analytic expression is given by Eq. (51) in which the parameters a and b are defined according to Eq. (41). For case 1, which is the only case we will examine here, the variables a and b is equal to $-ik_0$ respective $-k_0$. Approximating the Bessel with the far field approximation;

$$J_0(x) \approx \sqrt{\frac{2}{x\pi}} \cos\left(x - \frac{\pi}{4}\right), \tag{54}$$

the Bessel expression can be rewritten as follows

$$e^{-ikx} J_0(-kx) \approx \sqrt{\frac{-1}{2xk\pi}} \left(\cos\left(\frac{\pi}{4}\right) + \cos\left(2kx + \frac{\pi}{4}\right) + i\sin\left(\frac{\pi}{4}\right) - i\sin\left(2kx + \frac{\pi}{4}\right) \right). \tag{55}$$

From the above equation it is easy to see that the function oscillates around a value different from zero, and that value decreases with x, which coincides with the behaviour seen in Figure 2b.
In Figure 3a we can see a somewhat unexpected behaviour; the semi discrete kernel went down to zero every second step, and for the others it had a value twice as high as the continuous one. The semi-discrete SPE convolution kernel, given by Eq. (49), will now be used to verify this behaviour.

According to [4] a Legendre polynomial can be written as

$$P_n(\cos(\theta)) \approx \left(\frac{2}{n\pi\sin(\theta)}\right)^{1/2} \cos\left(n\theta + \frac{1}{2}\theta - \frac{1}{4}\pi\right), \tag{56}$$

and here cos(θ) is μ, defined by Eq. (33). Series developing the expression for μ, and neglecting the second order terms of α (α is zero for case 1, but we assume it to be small since Eq. (55) is singular there), leads to the relation

$$\mu \approx \frac{\alpha\Delta x}{2}. \tag{57}$$

Eq. (56) can, under the small angle assumption that $\cos\left(\frac{\pi}{2} - \frac{\alpha\Delta x}{2}\right) \approx \frac{\alpha\Delta x}{2}$, be written as

$$P_n\left(\frac{\alpha\Delta x}{2}\right) \approx \left(\frac{2}{n\pi}\right)^{1/2} \cos\left(n\left(\frac{\pi}{2} - \frac{\alpha\Delta x}{2}\right) - \frac{\alpha\Delta x}{4}\right), \tag{58}$$

which in turn can be approximated;

$$P_n\left(\frac{\alpha\Delta x}{2}\right) \approx \left(\frac{2}{n\pi}\right)^{1/2} \left[\cos\left(\frac{n\pi}{2}\right)\cos\left(\frac{n\alpha\Delta x}{2}\right) + \sin\left(\frac{n\pi}{2}\right)\sin\left(\frac{n\alpha\Delta x}{2}\right)\right]. \tag{59}$$

The semi discrete convolution kernel given by Eq. (49) can now, under the approximation

$$\left(\sqrt{\frac{C}{A}}\right)^n \approx i^n \left(1 + \frac{i\alpha\Delta x}{2}\right)^n \approx i^n e^{\frac{i\alpha\Delta x n}{2}}, \tag{60}$$

be written as

$$\frac{-4}{1+i}\sqrt{\frac{k_0\Delta x}{n\pi}} e^{\frac{i\alpha\Delta x n}{2}} * \begin{cases} \mathrm{Re}\left\{e^{\frac{i\alpha\Delta x n}{2}}\right\}, & If \quad n \quad even \\ i * \mathrm{Im}\left\{e^{\frac{i\alpha\Delta x n}{2}}\right\}, & If \quad n \quad odd \end{cases} \tag{61}$$

From the above equation, and with the fact in mind that α is zero, it is easy to verify the behavior in Figure 4, i.e. when n is odd the semi discrete SPE goes down to zero. Comparing the expression in Eq. (61) with the continuous kernel given by Eq. (48), it is seen that the amplitude (for those different from zero) of the semi discrete kernel is twice as big as the continuous, which also agrees with Figure 4.

5 Implementing the model

For the discretization of the continuous PE-models (10) and (11) we apply the Crank-Nicolson scheme [5]. Then in the range-independent case we obtain,

SPE:

$$\frac{1}{\rho_j}\frac{u_j^{n+1}-u_j^n}{\Delta x}=\frac{i}{4k_0}\left(\frac{1}{\rho_{j+\frac{1}{2}}}\frac{u_{j+1}^{n+1}-u_j^{n+1}}{\Delta z^2}-\frac{1}{\rho_{j-\frac{1}{2}}}\frac{u_j^{n+1}-u_{j-1}^{n+1}}{\Delta z^2}\right)+$$
$$+\frac{i}{4k_0}\left(\frac{1}{\rho_{j+\frac{1}{2}}}\frac{u_{j+1}^{n}-u_j^{n}}{\Delta z^2}-\frac{1}{\rho_{j-\frac{1}{2}}}\frac{u_j^{n}-u_{j-1}^{n}}{\Delta z^2}\right)+\frac{i\alpha_j}{2\rho_j}\left(u_j^{n+1}+u_j^n\right), \quad \textbf{(62)}$$

where $\alpha_j=\frac{k_j^2-k_0^2}{2k_0}$ and $\rho_{j\pm\frac{1}{2}}=\frac{1}{2}\left(\rho_j+\rho_{j\pm1}\right)$,

WAPE:

$$\frac{1}{\Delta x\Delta z^2}\left(\frac{u_{j+1}^{n+1}-u_j^{n+1}}{\rho_{j+\frac{1}{2}}}-\frac{u_j^{n+1}-u_{j-1}^{n+1}}{\rho_{j-\frac{1}{2}}}-\frac{u_{j+1}^{n}-u_j^{n}}{\rho_{j+\frac{1}{2}}}+\frac{u_j^{n}-u_{j-1}^{n}}{\rho_{j-\frac{1}{2}}}\right)+\frac{\beta_j}{\rho_j}\frac{u_j^{n+1}-u_j^n}{\Delta x}+$$
$$+i\frac{\chi_j}{2\rho_j}\left(u_j^{n+1}+u_j^n\right)+i\frac{\gamma_j}{\Delta z^2}\left(\frac{u_{j+1}^{n}-u_j^{n}}{\rho_{j+\frac{1}{2}}}-\frac{u_j^{n}-u_{j-1}^{n}}{\rho_{j-\frac{1}{2}}}\right)=0, \quad \textbf{(63)}$$

where $\beta_j=k_j^2+3k_0^{\,2}$, $\chi_j=2k_0(k_0^{\,2}-k_j^2)$ and $\gamma_j=-2k_0$. Now a tridiagonal equation system can be created, which needs to be solved for each step in x. The first and last equation in the system is created with help of the boundary conditions, i.e. the first one with help of the Dirichlet pressure release condition and the last with help of the boundary conditions created for the SPE and WAPE in Section 2.2.3 respective 2.2.6. The system then takes the form

$$\begin{bmatrix} a_1 & b_1 & 0 & \cdot & \cdot & \cdot & 0 \\ c_2 & a_2 & b_2 & \cdot & & & \cdot \\ 0 & c_3 & a_3 & b_3 & \cdot & & \cdot \\ \cdot & \cdot & \cdot & \cdot & \cdot & \cdot & \cdot \\ \cdot & & \cdot & \cdot & \cdot & \cdot & 0 \\ \cdot & & & \cdot & \cdot & \cdot & b_{J-1} \\ 0 & \cdot & \cdot & \cdot & 0 & c_J & -\dfrac{c_J D}{E} \end{bmatrix} \begin{bmatrix} u_1^{n+1} \\ u_2^{n+1} \\ u_3^{n+1} \\ \cdot \\ \cdot \\ \cdot \\ u_J^{n+1} \end{bmatrix} = \begin{bmatrix} d_1 u_1^n + e_1 u_2^n \\ d_2 u_2^n + e_2 u_3^n + f_2 u_1^n \\ d_3 u_3^n + e_3 u_4^n + f_3 u_2^n \\ \cdot \\ \cdot \\ d_{J-1} u_{J-1}^n + e_{J-1} u_J^n + f_{J-1} u_{J-2}^n \\ c_J \dfrac{F-R}{E} \end{bmatrix}$$

where the coefficients a, b, c, d, e and f are given by Eq. (62) and (63), for SPE respective WAPE. The first point, i.e. index 1, corresponds to the first point under the surface, and the point J is the one just below the z level where the DTBC is applied. The variables D, E, F and R are identified below by using Eqs. (39), (47) and the matching conditions given by Eqs. (14) and (15).

$$\left.\begin{aligned} \frac{u_1^{DTBC+} + u_0^{DTBC+}}{2} &= \frac{u_J^{DTBC-} + u_{J-1}^{DTBC-}}{2} \\ \frac{1}{\rho^{DTBC+}} \frac{u_1^{DTBC+} - u_0^{DTBC+}}{\Delta z^{DTBC+}} &= \frac{1}{\rho^{DTBC-}} \frac{u_J^{DTBC-} - u_{J-1}^{DTBC-}}{\Delta z^{DTBC-}} \end{aligned}\right\} \Rightarrow$$

SPE:

$$\frac{1}{\rho^{DTBC-}} \frac{u_J^{n+1} - u_{J-1}^{n+1}}{\Delta z^{DTBC-}} = \frac{1}{\rho^{DTBC+}} \frac{-4k_0}{\sqrt{A_{SPE\_xz}}} \sum_{k=0}^{n} l_{n-k} \left(\begin{aligned} &\frac{u_{J-1}^{k+1} - u_{J-1}^k + u_J^{k+1} - u_J^k}{2\Delta x} + \\ &-\frac{i\alpha}{4}\left(u_{J-1}^{k+1} + u_{J-1}^k + u_J^{k+1} + u_J^k\right) \end{aligned} \right) \quad \textbf{(64)}$$

WAPE:

$$\frac{1}{\rho^{DTBC-}} \frac{u_J^{n+1} - u_{J-1}^{n+1}}{\Delta z^{DTBC-}} = \frac{1}{\rho^{DTBC+}} \frac{i2\beta\Delta x}{\sqrt{A_{WAPE\_xz}}} \sum_{k=0}^{n} l_{n-k} \left(\begin{aligned} &\frac{u_{J-1}^{k+1} - u_{J-1}^k + u_J^{k+1} - u_J^k}{2\Delta x} + \\ &-\frac{i\chi}{4\beta}\left(u_{J-1}^{k+1} + u_{J-1}^k + u_J^{k+1} + u_J^k\right) \end{aligned} \right) \quad \textbf{(65)}$$

Rewriting the Eqs. (64) and (65),

$$Dp_J^{n+1} - Ep_{J-1}^{n+1} = -F + R, \quad \textbf{(66)}$$

one can for SPE identify the constants D, E, F and R as

$$D = \frac{\rho^{DTBC+}}{\rho^{DTBC-}} + \Delta z^{DTBC-} \frac{4k_0}{\sqrt{A_{SPE\_xz}}} l_0\left(\frac{1}{2\Delta x} - \frac{i\alpha}{4}\right),$$

$$E = \frac{\rho^{DTBC+}}{\rho^{DTBC-}} - \Delta z^{DTBC-} \frac{4k_0}{\sqrt{A_{SPE\_xz}}} l_0\left(\frac{1}{2\Delta x} - \frac{i\alpha}{4}\right),$$

$$F = -\Delta z^{DTBC-} \frac{4k_0}{\sqrt{A_{SPE\_xz}}} l_0\left(\frac{1}{2\Delta x} - \frac{i\alpha}{4}\right)\left(p_J^n + p_{J-1}^n\right) \text{ and}$$

$$R = -\Delta z^{DTBC-} \frac{4k_0}{\sqrt{A_{SPE\_xz}}} \sum_{k=0}^{n-1} l_{n-k} \left(\begin{array}{l} \frac{p_{J-1}^{k+1} - p_{J-1}^k + p_J^{k+1} - p_J^k}{2\Delta x} + \\ -\frac{i\alpha}{4}\left(p_{J-1}^{k+1} + p_{J-1}^k + p_J^{k+1} + p_J^k\right) \end{array} \right).$$

For WAPE they take the following form

$$D = \frac{\rho^{DTBC+}}{\rho^{DTBC-}} - \Delta z^{DTBC-} \frac{i2\beta\Delta x}{\sqrt{A_{WAPE\_xz}}} l_0\left(\frac{1}{2\Delta x} - \frac{i\chi}{4\beta}\right),$$

$$E = \frac{\rho^{DTBC+}}{\rho^{DTBC-}} + \Delta z^{DTBC-} \frac{i2\beta\Delta x}{\sqrt{A_{WAPE\_xz}}} l_0\left(\frac{1}{2\Delta x} - \frac{i\chi}{4\beta}\right),$$

$$F = \Delta z^{DTBC-} \frac{i2\beta\Delta x}{\sqrt{A_{WAPE\_xz}}} l_0\left(\frac{1}{2\Delta x} - \frac{i\chi}{4\beta}\right)\left(p_J^n + p_{J-1}^n\right) \text{ and}$$

$$R = \Delta z^{DTBC-} \frac{i2\beta\Delta x}{\sqrt{A_{WAPE\_xz}}} \sum_{k=0}^{n-1} l_{n-k} \left(\begin{array}{l} \frac{p_{J-1}^{k+1} - p_{J-1}^k + p_J^{k+1} - p_J^k}{2\Delta x} + \\ -\frac{i\chi}{4\beta}\left(p_{J-1}^{k+1} + p_{J-1}^k + p_J^{k+1} + p_J^k\right) \end{array} \right).$$

6 Source representations

When solving the system of equations in Chapter 5 for the first step, we need the initial conditions, u(0,z) (RHS). We shall assume that the source of the continuous model can be represented by a Dirac function at $(0,z_s)$, where z_s is the source depth. The simplest numerical analogue would be a spike of the height $1/\Delta z$ at one of the grid points in the vicinity of $(0,z_s)$.

This turned out to be a bad initial field. It introduced high frequency components, which remained within the solution domain despite the presence of a DTBC.

The next source is a Gaussian, first proposed as an initial field for the SPE by Tappert [1], which in the simplest form looks like

$$u(0,z) = Ae^{-\frac{(z-z_s)^2}{W^2}}, \tag{67}$$

where A is the amplitude of the source, W the source aperture defined as the 1/e-decay point, and z_s is the source depth. In [3] it is shown that through matching with a point-source solution in the farfield for the Helmholtz equation in homogeneous medium, the normalized Gaussian source take the form

$$u(0,z) = \sqrt{k_0}\,\tan(\theta_1) e^{-\frac{k_0^2}{2}(z-z_s)^2\tan^2(\theta_1)} e^{ik_0(z-z_s)^2\sin(\theta_2)}, \tag{68}$$

where θ_1 is the halfwidth of the source aperture defined below, and θ_2 is the beam tilt with respect to the horizontal, measured positive downward,

$$\tan^2(\theta_1) = \frac{2}{k_0^2 W^2}. \tag{69}$$

Note that the normally used Gaussian source is obtained through setting the beam tilt to zero and the halfwidth of the source aperture to 45°. Making the source in Eq. (68) applicable to the half-space case, i.e. the pressure is zero at the surface, a negative mirror source is placed above the surface. The Gaussian source now takes the form

$$u(0,z) = \sqrt{k_0}\,\tan(\theta_1)\left(e^{-\frac{k_0^2}{2}(z-z_s)^2\tan^2(\theta_1)} e^{ik_0(z-z_s)^2\sin(\theta_2)} - e^{-\frac{k_0^2}{2}(z+z_s)^2\tan^2(\theta_1)} e^{ik_0(z+z_s)^2\sin(\theta_2)} \right). \tag{70}$$

The third and last source used here is a Greene's source, which is a weighted Gaussian source with good wide-angle properties [3],

$$u(0,z) = \sqrt{k_0}\left(1.4467 - 0.4201 k_0^2 (z-z_s)^2\right) e^{-\frac{k_0^2(z-z_s)^2}{3.0512}}. \tag{71}$$

7 Model verification

In this Chapter the implemented model will be used to solve three benchmark examples, and the results are then compared with already existing solutions. The examples in question are; the Lloyd mirror, the Bucker waveguide and the Jensen-Kuperman wedge.

7.1 Matching the 2D solution to the 3D

To be able to compare with well know references, where cylindrical symmetry usually is used, the 2D solution have to be matched so it represents the 3D case. Solving the Helmholtz equation for a point source, for the 2 cases and comparing the solutions (see Appendix A) the following relation is achieved:

$$u_{3D} = u_{2D}\frac{1}{2}\sqrt{\frac{1}{2k_0 x\pi}}e^{-i\left(k_0 x+\frac{\pi}{4}\right)}. \tag{72}$$

The relation above implies that the correct 3D behavior is obtained if the 2D solution is divided with the square root of the range. When presenting results in ocean acoustics it is common practice to use transmission loss (TL), which for a normalized starting field can, for the 3D case, be calculated as

$$TL_{3D} = -20\log_{10}\frac{|u|}{\sqrt{x}}, \tag{73}$$

and in 2D it takes the following form

$$TL_{2D} = -20\log_{10}|u|. \tag{74}$$

7.2 Lloyd mirror

The Lloyd mirror case consists of a source in a half-infinite water volume. This implies that the acoustic field only interacts with the "smooth" water surface. Here the DTBC is applied at a depth of 100m, the density is set to 1000kg/m^3, the sound speed is 1500m/s, a source frequency of 100Hz and without damping. The source used in this case is the Gaussian given by Eq. (72), with a half-width opening angle of 45 degrees and zero beam tilt, placed at a depth of 30m. As one can see the Lloyd mirror is a very simple arrangement, and it's analytical solution is therefore possible to find. The analytical solution is obtained by using the method of mirror sources [6], i.e. summing the whole-space solutions for the source and its negative mirror,

$$u(r,z) = \frac{1}{4R_1\pi} e^{ik_0 R_1} - \frac{1}{4R_2\pi} e^{ik_0 R_2},$$

where $R_1 = \sqrt{r^2 + (z - z_s)^2}$ and $R_2 = \sqrt{r^2 + (z + z_s)^2}$. In the Figure 7 a 3D comparison between the analytical and numerical solutions is made.

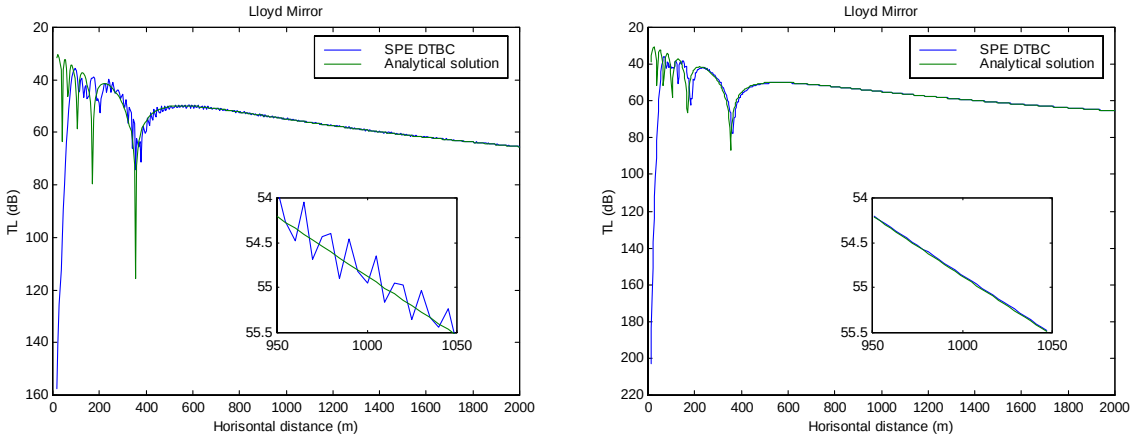

(a) (b)

Figure 7 Transmission losses at a depth of 90m for a source at 30m in a homogeneous water half-space, computed with the SPE approximation compared with the analytical solution. In the left picture (a) the SPE DTBC model uses dx=5m and dz=2m, and in the right (b) dx=3 and dz=1m.

Looking at Figure 7 (a) one can see that the solution obtained with the SPE DTBC model fits well with the analytical solution in the far field, though it has some artificial oscillations. The oscillations originate from the step size in x and z, and can be shown to disappear if reducing the size of the steps, see Figure 7 (b).

7.3 Bucker Wave Guide

In this example there is a horizontal bottom at a depth of 240m, and a Gaussian source with a frequency of 100Hz at a depth of 30m. The density in the water is 1000kg/m^3 and in the bottom 2100kg/m^3. The sound speed in the bottom is 1505m/s, and in the water it is given by the sound speed profile; $c_b = 1498 + |120 - z|/60$ m/s, see Figure 8. The DTBC is applied immediately at the water-bottom interface, i.e. at a depth of 240m. The 3D transmission loss at a depth of 90m for the SPE DTBC model is displayed in Figure 9, and it coincides with the results obtained in several sources ([2], [3] and [7]).

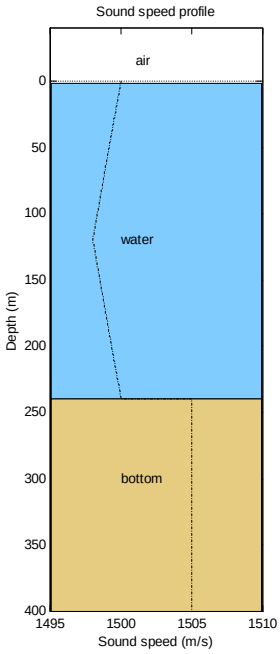

Figure 8 Sound speed profile for the Bucker wave guide.

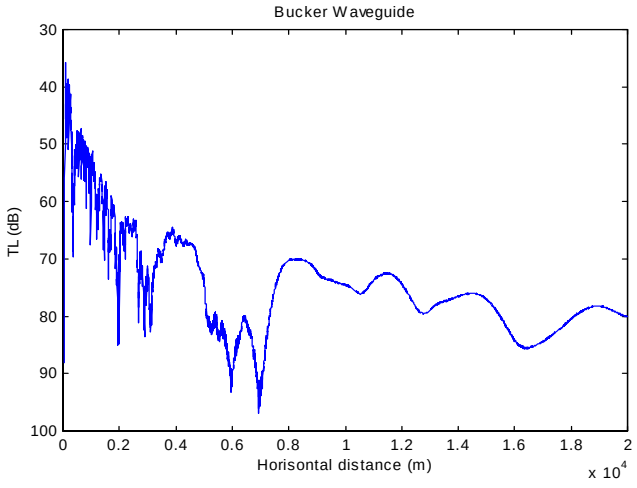

Figure 9 Transmission losses at a depth of 90m for a source at 30m in a homogeneous water half-space, computed with the SPE approximation.

7.4 The Jensen-Kuperman Wedge

Here, in this Section bottom is at a depth of 200m for the first 5000m and thereafter the water depth is linearly decreased down to 0m at the range of 12500m, see Figure 10. The source is placed at a depth of 180m, and close to the bottom. Therefore the Greene's source, given by Eq. (71), is used, due to its good wide-angle properties. The frequency is set to 25Hz, the density in the water is 1000kg/m^3 and in the bottom 1200kg/m^3. The sound velocity in the water is 1500m/s and in the bottom 1700m/s. There is no damping in the water but in the bottom there is a natural damping of 0.5dB/λ. Placing the DTBC at the depth of 600m, i.e. 400m down into the bottom, results in Figure 19 of the transmission loss in 2D.

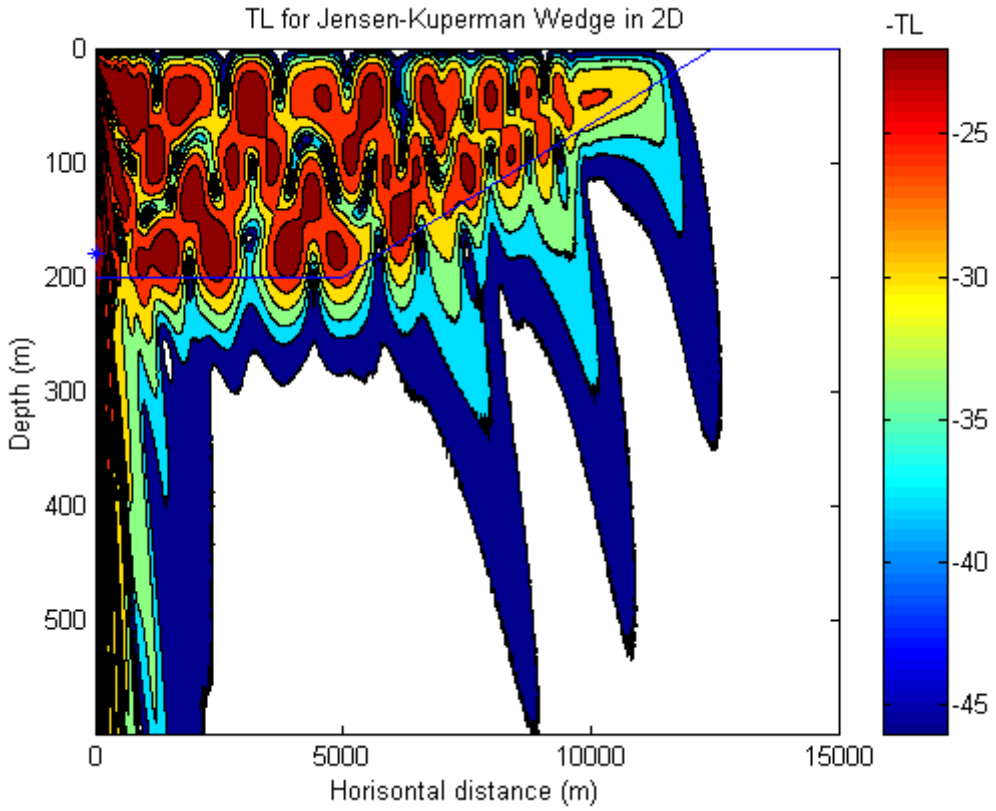

Figure 10 Transmission losses in a wedge for a Greene's source at a depth of 180 m, calculated with the WAPE DTBC. The blue line represents the water-bottom boundary.

The transmission loss in Figure 10 agrees well with the results presented in [3], and we see the three "well known fingers" in the bottom slope.

8 Comparison with artificial absorbing layers

A common way to truncate the computational domain in the depth direction is to add an artificial absorbing layer with a thickness of 10-15 wavelengths. Usually it has the same density and sound velocity as the homogeneous semi-infinite bottom, while the absorption is significantly larger than the natural one. The layer is terminated by a pressure release condition. In order to prevent back reflections all waves must be sufficiently damped until this boundary condition can be applied. It is also desired to keep the absorbing layer as thin as possible to save computational time. It turns out that the damping should be increased gradually. The construction of a suitable damping profile leads to an optimization problem in which the allowed amount of back reflection is a constraint. Typically such a profile has a depth of 10-15 wavelengths over which the absorption increases in a nonlinear way. We have used the same code as in [14] to generate quasi-optimal absorption profiles. A simpler approach is to let the absorption increase linearly from the natural value to 10dB/λ over 10 wavelengths. We have compared these two alternatives with the use of DTBC's. A linear profile with the same thickness as the computed profile is also used, this to get a fair comparison between the linear and the computed profile.
The implementation of the different models was made in the program MatLab on a PC with an Intel Pentium III processor 500Mhz and a RAM memory of 128Mb. Below, the damping

profiles used for the Lloyd mirror case are displayed. There is a difference in thickness, between the damping profiles in the three cases, which arises from that one prefers to denote the layer thickness in a specific number of wave lengths. The main behavior of the damping profiles is given by Figure 11, though the gradient for the linear profiles changes from case to case since the damping is 10dB/λ over some layer thickness. The input variable that sets the level of allowed reflections, in the program that computes the "favorable" damping layer, is set to 50dB.

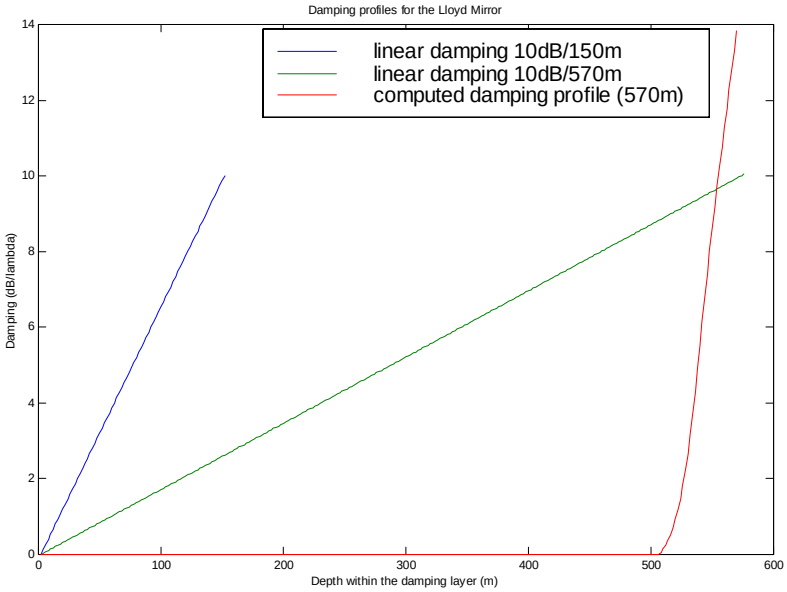

Figure 11 Damping profiles used for the Lloyd mirror case. The blue line corresponds to a layer thickness of 10 wave lengths, the green answers to a 570m thick layer which originates from the thickness of the computed profile (the red line).

8.1 Evaluating the Lloyd mirror case

Here the Lloyd mirror example, defined in Section 7.2, will be used to compare the SPE DTBC model efficiency and correctness versus damping layers. Three different damping profiles are used; a 10 wavelength thick layer (150m), a computed damping profile and one that has the same thickness as the computed profile (570m). The TL at a depth of 90m is displayed in Figure 12 for the linear profiles, the computed profile, the SPE DTBC model and the analytical solution. It is easy to see that the SPE DTBC model is preferable vs. the damping layers, when it comes to correctness. The SPE coincides well with the analytical solution, while the computed damping profile works up to a 6500m range were it highly overestimates the TL and thereafter behaves bad. The linear damping profiles don't behave as hysterical, but departs at a closer range from the analytical solution. From Figure 12 it can be seen that the thicker damping layers, and therefore a smaller damping gradient, the closer to the analytical solution we get. The linear damping profiles though never get close to the correctness of the SPE model.

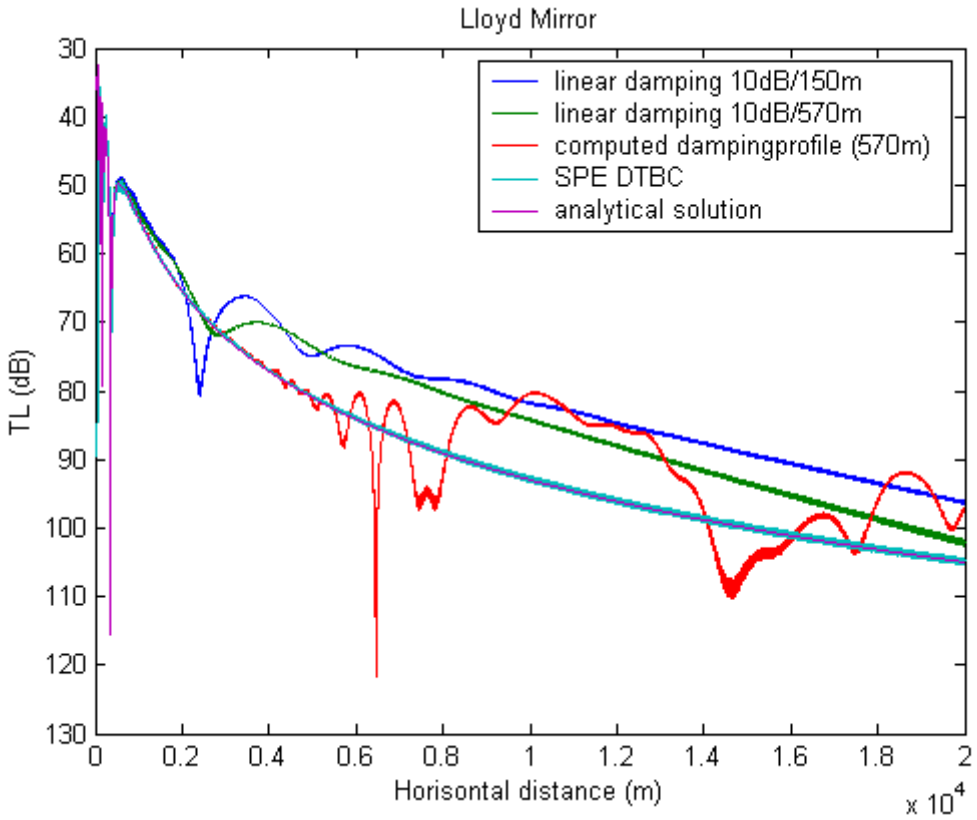

Figure 12 Comparison in TL, at a depth of 90m for the Lloyd mirror case, between the SPE DTBC model, the analytical solution and the damping layers.

In the table below the time elapsed for the respective model is shown for the horizontal range of 20000m, and the water column is truncated at a depth of 100m.

Table 2 Elapsed time for the different simulation models for the Lloyd mirror case.

	Number of simulations	Mean value (s)	Standard deviation (s)
SPE DTBC (50*4000 points)	10	45	1
Linear 10 lambda (125*4000 points)	10	85	2
Computed profile (334*4000 points)	5	434	4

From the figures in Table 2 it is seen that the SPE model is the most time efficient alternative, almost twice as fast (1.9) as the 10 wavelengths thick damping layer, and 9.6 as fast as the computed profile.

8.2 Evaluating the Bucker-wave guide

In this section we will examine the efficiency and correctness for the different models for the Bucker wave-guide, defined in section 7.3. Below in Figure 13 the TL is plotted at a depth of 90m for the SPE model and the same damping profiles as for the Lloyd mirror case above. As seen from the picture the solution obtained with the computed profile follows the SPE solution better then the linear profiles except at the range just above 16000m, where it highly overestimates the TL. The linear damping profiles get closer to the SPE solution with thickness, but can never compete with the SPE.

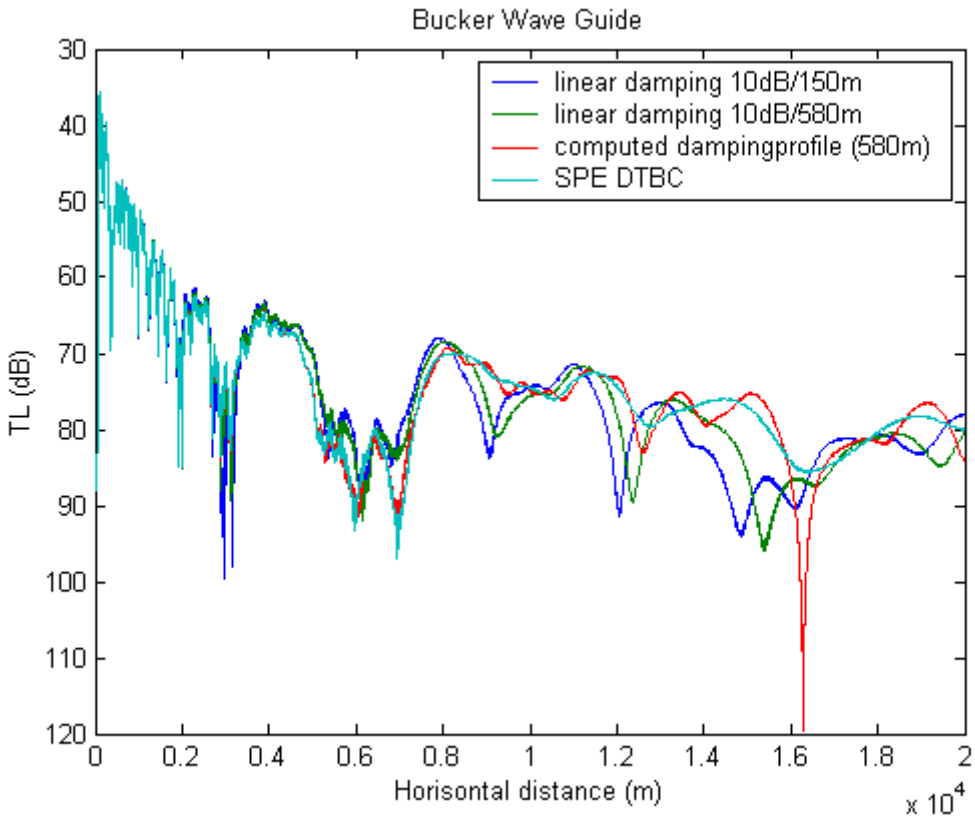

Figure 13 Comparison in TL, at a depth of 90m for the Bucker wave-guide, between the SPE DTBC model and the different damping layers.

The time it took to solve the physical domain of range 20000m and depth of 240m (cut at the water bottom interface) is shown in table 3. It can be seen that the SPE is approximately 1.8 times faster than the 10 wavelengths thick layer, and 6.3 times more efficient than the compute profile.

Table 3 Elapsed time for the different simulation models for the Barker wave-guide.

	Number of simulations	Mean value (s)	Standard deviation (s)
SPE DTBC (120*4000 points)	10	99	1
Linear 10 lambda (195*4000 points)	10	174	2
Computed profile (407*4000 points)	5	621	4

8.3 Evaluating the Jensen-Kuperman Wedge

Here for the Jensen-Kuperman wedge, defined in Section 7.4, the physical domain has the range 15000m and a depth of 200m. The 2D TL in Figure 14 is taken at a depth of 100m, for the SPE model. A linear damping layer of the thickness 10 wavelengths and the computed damping profile is used. As seen, the models coincide well, this due to the rather thick damping layers and a natural damping in the bottom. The thickness originates from the "low" frequency (25Hz), leading to a large wavelength.

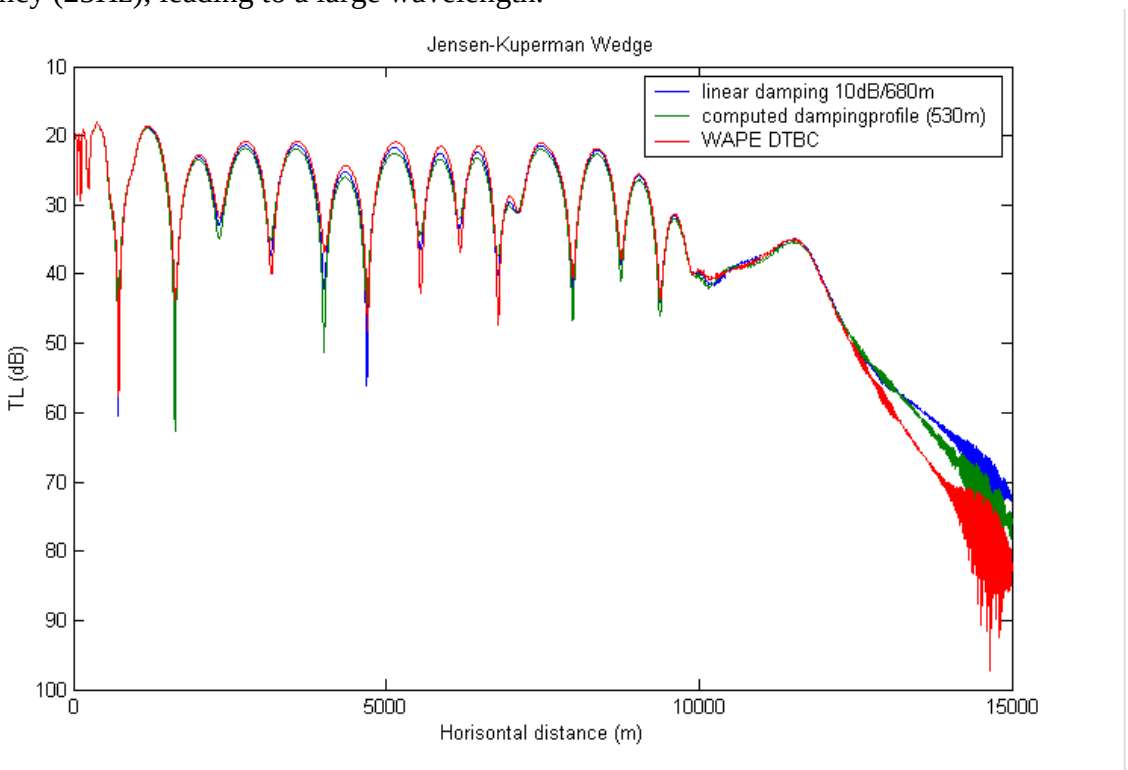

Figure 14 Transmission losses (2D) at a depth of 100 m for propagation in a wedge, calculated with a linear damping profile (0 to 10 dB over 10 wavelengths), a computed damping profile and with the WAPE DTBC.

In Table 4 we can see that the WAPE DTBC model is much more time effective than the linear model, with the thickness of 10 wavelengths. Due to the natural damping in the bottom, the damping layer with the computed damping profile, becomes thinner and therefore faster then the linear one.

Table 4 Elapsed time for the different simulation models for propagation in a wedge.

	Number of simulations	Mean value (s)	Standard deviation (s)
WAPE DTBC (100*3000 points)	10	59	1
Linear 10 lambda (439*3000 points)	10	536	5
Computed profile (365*3000 points)	10	381	4

9 Conclusions

The DTBC models, implemented in this thesis, showed to be much more time efficient than the so far used damping layer method, and also give a much more exact solution. Especially in cases without damping the DTBC gives a crucial correctness vs. damping layers. Since the DTBC is the correct boundary condition, as far as the approximations made are valid, the DTBC model gives a much more accurate solution and should therefore be used whenever a more exact solution is needed.

The DTBC boundary condition contains a convolution involving all the boundary points in the past range, which may be unnecessary. So as further work an algorithm cutting off this convolution tail, might make the DTBC model even more efficient. As an example it can be mentioned that, for the Bucker wave-guide with the range of 20000m and depth of 240m, the summing of the convolution terms took around 10-15% of the elapsed time.

The time figures obtained in this paper don't give full credit to MatLab, since some routines that needed too much memory had to be written in MatLab non-optimal code. So the estimated computational values obtained are not final, but give a hint of the superiority of the DTBC vs. the damping layers.

In this report we only used uniform step sizes, and since it is preferable to have adaptive grid spacing, there is possible to further optimize the software in many areas.

Acknowledgement

I thank my supervisor at FOI Leif Abrahamsson for lots of help to get insight into the world of the underwater acoustics. His sacrificing work helping me to eliminate program bugs, verifying calculations and his positive criticism when writing this thesis has been of great value.

References

[1] Hardin, R.H and Tappert, F. D. (1973). Applications of the split-step Fourier method to the numerical solution of nonlinear and variable coefficient wave equations. *SIAM* Rev. 15, 423.

[2] Arnold, A. and Ehrhardt, M. (1998). Discrete transparent boundary conditions for wide angle parabolic equations in underwater acoustics. *Journal of computational physics*, 145 (2), 611-638.

[3] Jensen, F. B., Kuperman, W. A., Porter, M. B. and Schmidt, H. (1994). *Computational ocean acoustics.* NY: AIP Press. ISBN 1-56396-209-8.

[4] Olver, F. W. J. (1974). *Asymptotics and special functions*. NY and London: Academic Press. ISBN 0-12-525850-X.

[5] Garcia, A. L. (2000). *Numerical methods for physics*. 2nd edition. New Jersey: Prentice-Hall. ISBN 0-13-906744-2.

[6] Wangsness, R. K. (1986). *Electromagnetic fields.* 2nd edition. NY: John Wiley & Sons. ISBN 0-471-81186-6.

[7] PE Workshop 2: Proceedings of the second parabolic equation workshop (1993). Ed. by Chin-Bing, S. A., King, D. B., Davis, J. A. and Evans R. B. Naval research laboratory. ISBN 7181-93-0001.

[8] Råde, L. and Westergren, B. (1995). *Beta; Mathematics handbook.* 3rd edition.Lund: Studentlitteratur. ISBN 91-44-25053-3.

[9] Brekhovskikh, L. and Lysanov, Y. (1982). *Fundamentals of Ocean Acoustics*. Berlin: Springer-Verlag.

[10] Abrahamsson, L., Andersson, L., Karasalo, I. and Sundström, S. (1995). JEPE – a PE code for range-dependent fluid media: 10th Scandinavian Symposium in Physical Acoustics. University of Bergen, Norway. 1-3.

[11] Karasalo, I. and Sundström, A. (1996). JEPE – a high-order PE-model for range-dependent fluid media: Proceedings of the 3rd European Conference on Underwater Acoustics. Heraklion, Crete, Greese. 189-194.

[12] Andersson, B. L. (1998). JEPE-S: a PE code for wave propagation in range-dependent fluid solid media. Technical report FOA-R—98-00979-409—SE.

[13] Abrahamsson, L. and Andersson, B. L. (2000). Identification of seabed geoacoustic parameters from transmission loss data. Methodology report FOA-R-00-01752-409—SE.

[14] Sundström, A. (2000). A stable PE model for wave propagation in fluid-solid media. Scientific report FOA-R-00-01741-409—SE.

[15] Papadakis, J. S. (1982). Impedance Formulation of the Bottom Boundary Condition for the Parabolic Equation Model in Underwater Acoustics, NORDA Tech. Note 143.

[16] Dalrymple, R. A. and Martin, P. A. (1992). Perfect boundary conditions for parabolic water-wave models. Proc. R. Soc. London 437, 41-54.

[17] Sherman, W. M. (1991). A generalized impedance method for application of the parabolic approximation to underwater acoustics. J. Acoust. Soc. Am. 90 (1).

Appendix A: 2D vs. 3D

In a homogenous medium the SPE take the form

$$\frac{\partial u}{\partial x} = \frac{i}{2k_0}\frac{\partial^2 u}{\partial z^2}, \qquad x \geq 0 \qquad \textbf{A. 1}$$

Fourier transforming the SPE for a Dirac function as the initial field,

$$\frac{\partial \hat{u}(x,k_z)}{\partial x} = \frac{-i}{2k_0}k_z^2\hat{u}(x,k_z), \qquad \textbf{A. 2}$$

and the initial condition is given by

$$\hat{u}(0,k_z) = e^{-ik_z z_0}, \qquad \textbf{A. 3}$$

the solution is given by

$$\hat{u}(x,k_z) = e^{-i\frac{k_z^2}{2k_0}x - ik_z z_s}. \qquad \textbf{A. 4}$$

Inverse transforming the solution gives:

$$u(x,z) = \frac{1}{2\pi}\int_{-\infty}^{\infty} e^{-i\frac{k_z^2}{2k_0}x - ik_z z_s + ik_z z}\,dk_z = \frac{1}{2\pi}e^{i\frac{k_0(z-z_s)^2}{2x}}\int_{-\infty}^{\infty} e^{-i\frac{x}{2k_0}\left(k_z - \frac{k_0}{x}(z-z_s)\right)^2}\,dk_z \qquad \textbf{A. 5}$$

Substitute

$$t = \sqrt{\frac{x}{2k_0}}\left(k_z - \frac{k_0}{x}(z - z_s)\right)$$

$$dt = \sqrt{\frac{x}{2k_0}}dk_z$$

gives

$$u(x,z) = \frac{1}{2\pi}\sqrt{\frac{2k_0}{x}}e^{i\frac{k_0(z-z_s)^2}{2x}}\underbrace{\int_{-\infty}^{\infty} e^{-it^2}\,dt}_{=e^{-i\pi/4}\sqrt{\pi}} = \sqrt{\frac{k_0}{2x\pi}}e^{i\frac{k_0(z-z_s)^2}{2x} - i\frac{\pi}{4}}. \qquad \textbf{A. 6}$$

The 3D solution in cylindrical co-ordinates, assuming azimuthal symmetry, for the Helmholtz equation is

$$u(r,z)=\frac{1}{4R\pi}e^{ik_0R}, \qquad \textbf{A. 7}$$

where R is defined as; $R=\sqrt{r^2+(z-z_s)^2}$. Only being interested in the far field, the above equation can be approximated as;

$$u(r,z)=\frac{1}{4r\pi}e^{ik_0r+i\frac{k_0(z-z_s)^2}{2r}}. \qquad \textbf{A. 8}$$

Comparing the 2D and 3D solutions, given by equation A.6 and A.8, the following relation is obtained:

$$u_{3D}=u_{2D}\frac{1}{2}\sqrt{\frac{1}{2k_0x\pi}}e^{-i\left(k_0x+\frac{\pi}{4}\right)}. \qquad \textbf{A.9}$$